



# Biotinylated HPMA centered polymeric nanoparticles for Bortezomib delivery

Sarita Rani<sup>a</sup>, Rakesh K. Sahoo<sup>a</sup>, Kartik T. Nakhate<sup>b</sup>, Ajazuddin<sup>b</sup>, Umesh Gupta<sup>a,\*</sup>

<sup>a</sup> Department of Pharmacy, School of Chemical Sciences and Pharmacy, Central University of Rajasthan, Bandarsindri, Ajmer, Rajasthan 305817, India

<sup>b</sup> Rungta College of Pharmaceutical Sciences and Research, Kohka-Kurud Road, Bhilai, Chhattisgarh 490024, India



## ARTICLE INFO

### Keywords:

HPMA (N-2-hydroxypropyl methacrylamide)  
PLA (poly lactic acid)  
Biotin (BT)  
Polymeric nanoparticles (PNPs)  
Bortezomib (BTZ)  
Breast Cancer

## ABSTRACT

Bortezomib (BTZ) is a proteasome inhibitor as approved by US FDA for the treatment of multiple myeloma. It exhibits significant anti-cancer properties, against solid tumors; but lacks aqueous solubility, chemical stability which hinders its successful formulation development. The present study is an attempt to deliver BTZ using N-(2-hydroxypropyl) methacrylamide (HPMA) based copolymeric conjugates and biotinylated PNPs in an effective manner. Study describes a systematic synthetic pathway to synthesize functional polymeric conjugates such as HPMA-Biotin (HP-BT) HPMA-Polylactic acid (HPLA) and HPMA-PLA-Biotin (HPLA-BT) followed by exhaustive characterization both spectroscopically and microscopically. Our strategy yielded polymeric nanoparticles (PNPs) of narrow size range of  $199.7 \pm 1.32$  nm. Release studies were performed at pH 7.4 and 5.6. PNPs were 2-folds less hemolytic ( $p < 0.0001$ ) than pure drug. BTZ loaded PNPs of HPLA-BT demonstrated significant anti-cancer activity against MCF-7 cells.  $IC_{50}$  value of these PNPs was  $56.06 \pm 0.12$  nM, which was approximately two folds less than BTZ ( $p < 0.0001$ ). Cellular uptake study confirmed that higher uptake of formulations might be an outcome of biotin surface tethering characteristics that enhanced selectivity and targeting of formulations efficiently. *In vivo* pharmacokinetics evidenced increased bioavailability ( $AUC_{0-t_{\infty}}$ ) of DL-HPLA-BT PNPs (drug loaded) than BTZ with an improved half-life. Overall the developed PNPs led to the improved and effective BTZ delivery.

## 1. Introduction

In 1970s, Ringsdorf first highlighted the use of polymers as a therapeutic agent. Since then, plentiful of literature has been published on polymeric drug delivery (Ringsdorf, 1975). Polymeric conjugates are an astounding approach for targeted delivery of drugs at tumorous site. These can mask and control release of the bio-actives at diseased site. The breakthrough outcome was witnessed when the first polymer entered in the clinical trials (Vasey et al., 1999). Later on, poly-ethylene-glycol (PEG) based conjugates of proteins (Baka et al., 2006), antibodies (Veronese and Pasut, 2005) and polymeric micelles of encapsulated or conjugated drugs also entered in various clinical phases of evaluation. Conjugated polymer-based drug delivery through a nanoparticulate approach such as polymeric nanoparticles (PNPs), micelles, liposomes, and dendrimers etc. can efficiently deal with solubility and instability issues. PNPs are colloidal particles in size range of 10–1000 nm with a potential of prolonged distribution of drugs in the

blood (Elsabahy and Wooley, 2012). PNPs have a high degree of selectivity based on size and can deliver the conjugated molecules to the site of action.

Breast cancer is the second foremost cause of death worldwide among all the subtypes of cancers (Bray et al., 2018). Despite the advanced chemotherapy that improved the life span of cancer patients, the mortality rate of cancer had not decreased significantly. The reason sought to be the vague targeting and cytotoxic effects of drugs, which limits as well as hampers the positive effects of chemotherapy. ER-positive subtype is the most commonly diagnosed breast cancer (70%) in women (Pearce and Jordan, 2004). Bortezomib (BTZ) is a proteasome inhibitor, approved by US FDA (Food and Drug Administration) in 2003 for the treatment of multiple myeloma and have showed outstanding results for solid tumor treatment as a single agent or in combination therapy (Chen et al., 2011; Papandreou et al., 2004). BTZ revealed some extraordinary outcomes against ER-positive breast cancer recently (Maynadier et al., 2016; Thaler et al., 2017; Xia et al., 2018), but the

**Abbreviations:** HPMA, N-2-hydroxypropyl methacrylamide; PLA, Poly lactic acid; BTZ, Bortezomib; BT, Biotin; PNPs, Polymeric nanoparticles; FITC, Fluorescein isothiocyanate

\* Corresponding author.

E-mail address: [umeshgupta@curaj.ac.in](mailto:umeshgupta@curaj.ac.in) (U. Gupta).

<https://doi.org/10.1016/j.ijpharm.2020.119173>

Received 7 January 2020; Received in revised form 16 February 2020; Accepted 21 February 2020

Available online 22 February 2020

0378-5173/ © 2020 Elsevier B.V. All rights reserved.

low aqueous solubility, instability, and poor penetration in tumor cells are the major drawbacks (Wei et al., 2010). Su et al. explored the catechol conjugated polymers for BTZ drug delivery for breast cancer cells such as MDA MB-231, MCF-7. Results suggested that the prepared catechol system can be beneficial in cancer therapy (Su et al., 2011). Medel and coworkers prepared curcumin and BTZ loaded nanoparticles and observed the synergistic effect of curcumin and BTZ nanoparticles against solid tumor (Medel et al., 2017).

HPMA [N-(2-hydroxypropyl) methacrylamide], co-polymer has been widely explored for polymeric-drug conjugated delivery by Duncan in the past (Duncan, 2009). HPMA, a hydrophilic copolymer was supposed to enhance the aqueous solubility of hydrophobic drugs. HPMA has gained much attention as its first polymeric conjugate (FCE28068) entered in the clinical trials (Seymour et al., 2009). Considering attractive characteristics of HPMA it was selected as a hydrophilic carrier in the present work. PLA (poly-L-lactic acid) was preferred because of its ability to encapsulate the hydrophobic drug(s) into the intended PNPs core. PLA has biocompatibility and biodegradability properties which are fruitful for drug delivery applications. Barz et al. reported paclitaxel loaded HPMA polymeric micelles and studied their intracellular uptake and localization in HeLa cells (Human cervix adenocarcinoma cells) (Barz et al., 2012). Surprisingly, only few reports based on HPLA conjugation are reported yet (Barz et al., 2012). Hitherto, none of those reported a combined ester and amide linkage approach with biotin as a targeted molecule for developing PNPs. PNPs have some advantages in drug delivery system. Large sized particles can be easily engulfed by reticular endothelial cells (Senior et al., 1985) but this shortcoming can be overcome by developing a tumor specific nanoparticulate system. Significant drug loading is also expected to meet the requirement of suppression of cell proliferation and eventually to kill cancerous cells/tissue. Cancer cells usually have a hunger for some vitamins and receptors (Maiti et al., 2013). Biotin receptors are highly over expressed in certain cancer subtypes such as breast, lung, ovarian etc. in comparison to normal cells (Kue et al., 2016). This made our basis of using biotin as ligand in the intended nanoparticles of the present study. Among various vitamins, biotin draws special attention as it is being uptaken more rapidly by cancer cells than the normal cell (Ren et al., 2015).

Present study is based on the conjugation of different copolymers with biotin as a targeting ligand to examine the effect of biotinylated conjugates v/s non-biotinylated conjugates against breast cancer cells. The first objective of this study was to explore the capability of HPMA to enhance aqueous solubility of poorly soluble drug, BTZ. Therefore encapsulation of BTZ was achieved in HPMA based PNPs to enhance drug solubility. The second one was to explore BTZ applicability for solid tumors as BTZ showed remarkable anti-cancer activity against human breast cancer cell lines such as MCF-7 (Maynadier et al., 2016; Thaler et al., 2017; Xia et al., 2018) MDA-MB 231 (Su et al., 2011; Medel et al., 2017) and MDA-MB 268 (Shen et al., 2015). Third one was tumor-specific delivery of BTZ through biotinylated HPMA and PLA based PNPs It was also envisaged that conjugation with HPMA can potentiate drug payload and enhance the blood residence time of BTZ which in-turn would improve the overall bioavailability of BTZ.

## 2. Materials and methods

### 2.1. Materials

Methacryloyl chloride and aminopropanol-2-ol were procured from Alfa-Aesar Pvt. Ltd. India. Anhydrous sodium carbonate, anhydrous sodium sulfate, dry dichloromethane (DCM), acetone, methanol (MeOH), thionyl chloride ( $\text{SOCl}_2$ ), chloroform, dimethyl sulfoxide (DMSO), tetrahydrofuran (THF), and triethylamine (TEA) were purchased from TCI Chemicals Pvt. Ltd. India. PLA (Mn 10000–18000  $\text{g}\cdot\text{mol}^{-1}$ ) was a gift sample from Evonik Industries. Biotin, 4-dimethyl aminopyridine (DMAP), MTT (3-(4,5-

dimethylthiazol-2-yl)-2,5-diphenyl tetrazolium bromide), FITC (fluorescein isothiocyanate), DMEM (Dulbecco's Modified Eagle Medium), FBS (fetal bovine serum), streptomycin-penicillin, trypsin EDTA, dialysis membrane-50 and 150 were purchased from HiMedia. All the chemicals were used as such without any further purification. N, N-dicyclohexyl carbodiimide (DCC), 1-ethyl-3-(dimethylaminopropyl) carbodiimide (EDC), polyvinyl alcohol (PVA), lecithin, disodium hydrogen phosphate, potassium dihydrogen phosphate, tetrahydrofuran (THF), sodium hydroxide, sodium chloride, and ethanol were obtained from CDH, India. TLC plates were procured from Merck, India. Whatman filter papers and syringe filters were procured from Rankem, India. All the other reagents were of analytical grade with highest purity.

### 2.2. Synthesis and characterization polymeric conjugates

#### **Synthesis of HPMA (N-2-hydroxypropylmethacrylamide), HPMA-Biotin (HP-BT), HPMA-PLA (HPMA-poly-L-lactic acid; HPLA) and HPLA-Biotin (HPLA-BT)**

##### 2.2.1. HP-BT (N-2-hydroxypropylmethacrylamide-Biotin or HPMA-Biotin)

The co-polymer, HPMA was synthesized according to a previously reported literature (Chytil et al., 2010). HPMA (HP) and biotin (BT) were conjugated using DCC/DMAP coupling reaction (Fig. 1). Briefly, HPMA (10 mg) was dissolved in methylene chloride, then added in to the biotin (BT) solution (25.44 mg in DMSO) followed by addition of DCC. After 20 min, DMAP (dissolved in DCM) was added slowly to the reaction mixture and reaction time allowed was 24 h. TLC was performed initially to confirm the completion of reaction. The crude product was vacuum dried and kept in dialysis bag after dissolving in distilled water. The whole assembly was stirred in distilled water for 2 days to remove DMAP. The external solvent (water) was replaced after 12 h timely. A brown colored product was dried and a yield of 86% was calculated. The conjugate was characterized at each step by FT-IR, and NMR spectroscopy Fig. S1.

##### 2.2.2. HPLA (HPMA-Poly-L-lactic acid)

HPMA was conjugated to PLA according to the reported procedure (Upadhyay et al., 2017). Poly-L-lactic acid (PLA) (500 mg, 0.05 mmol) was dissolved in DCM (5 mL) with HPMA (7.1 mg, 0.05 mmol) in the excess of DCC (10.31 mg, 0.05 mmol). After 20 min, DMAP (6.1 mg, 0.05 mmol) was added to the reaction mixture. The reaction was allowed to proceed overnight. The conjugate was dialyzed using dialysis membrane for 24 h to remove DMAP. HPLA co-polymer was characterized by FT-IR (Fig. 2) using KBr pellet method (Perk, M/s Perkin Elmer Co., Waltham, Massachusetts, USA) and  $^1\text{H}$  NMR spectra were recorded in Bruker Ascend 500 MHz NMR spectrometer (Switzerland) using  $\text{CDCl}_3$  as solvent.

##### 2.2.3. HPLA-BT (HPMA-Poly-L-lactic acid-biotin conjugate)

Biotin (BT) (100 mg) was dissolved in dry DCM (5 mL) in RBF and kept at 0 °C. Thionyl chloride (59.38  $\mu\text{L}$ ) was added dropwise into the above solution. Thereafter, the reaction was transformed at 60 °C for 4–6 h. On completion of reaction, flask was cooled at room temperature and a solid yellow brown colored product was obtained. The product was washed three times with chilled DCM and vacuum dried (Hou et al., 2017). The product was immediately used for the next reaction. This biotin acylchloride (BT-Cl) intermediate was vacuum dried and further conjugated to HPLA. In the next step, HPLA (207 mg) was dissolved in dry DCM and kept for stirring at 0 °C. Then, tertiary amine ( $\text{Et}_3\text{N}$ ) was added to the reaction dropwise. Later, dry THF was added in the reaction mixture and reaction was allowed to proceed in cool condition and inert atmosphere for 18–20 h (Getlik et al., 2013; Goodreid et al., 2014). Subsequently, the product was dissolved in cold DCM (dichloromethane) and dried. The obtained product was washed with chilled DCM to remove the remaining traces of unreacted/

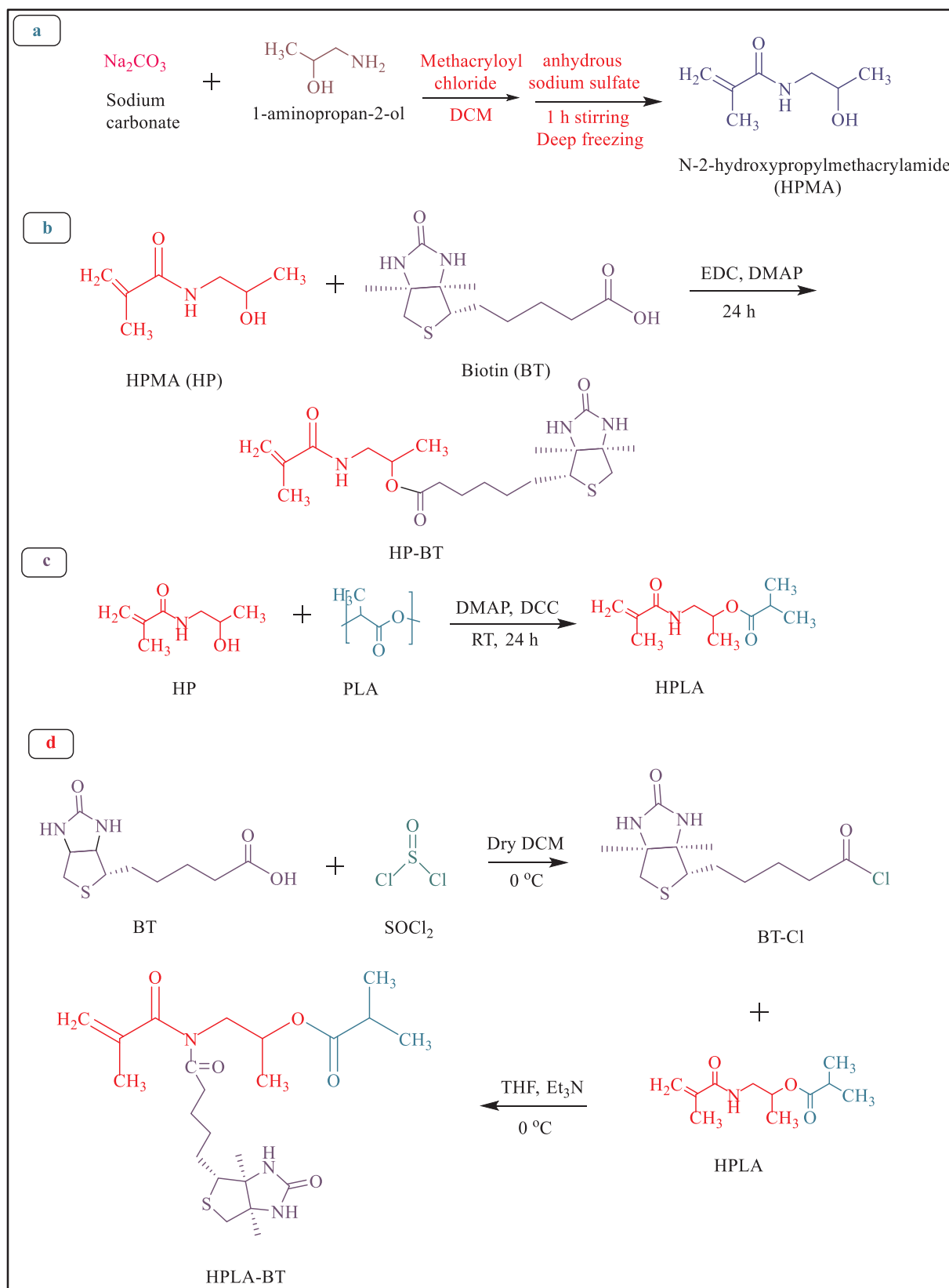


Fig. 1. Synthesis schemes of; (a) HPMA (b) HPMA-Biotin (HPBT) (c) HPMA-PLA (HPLA), and (d) HPMA-PLA-Biotin (HPLA-BT).

unmodified HPLA. The co-polymeric conjugate (HPLA-BT or HPMA-PLA-BT conjugate) (Fig. 1) was obtained as yellow color solid. Finally, the product was characterized by  $^1\text{H}$  and  $^{13}\text{C}$  NMR spectroscopy (Fig. 3).

### 2.3. Preparation of HP-BT, HPLA, HPLA-BT polymeric nanoparticles (PNPs)

The prepared polymeric conjugates (HPBT, HPLA, HPLA-BT) were

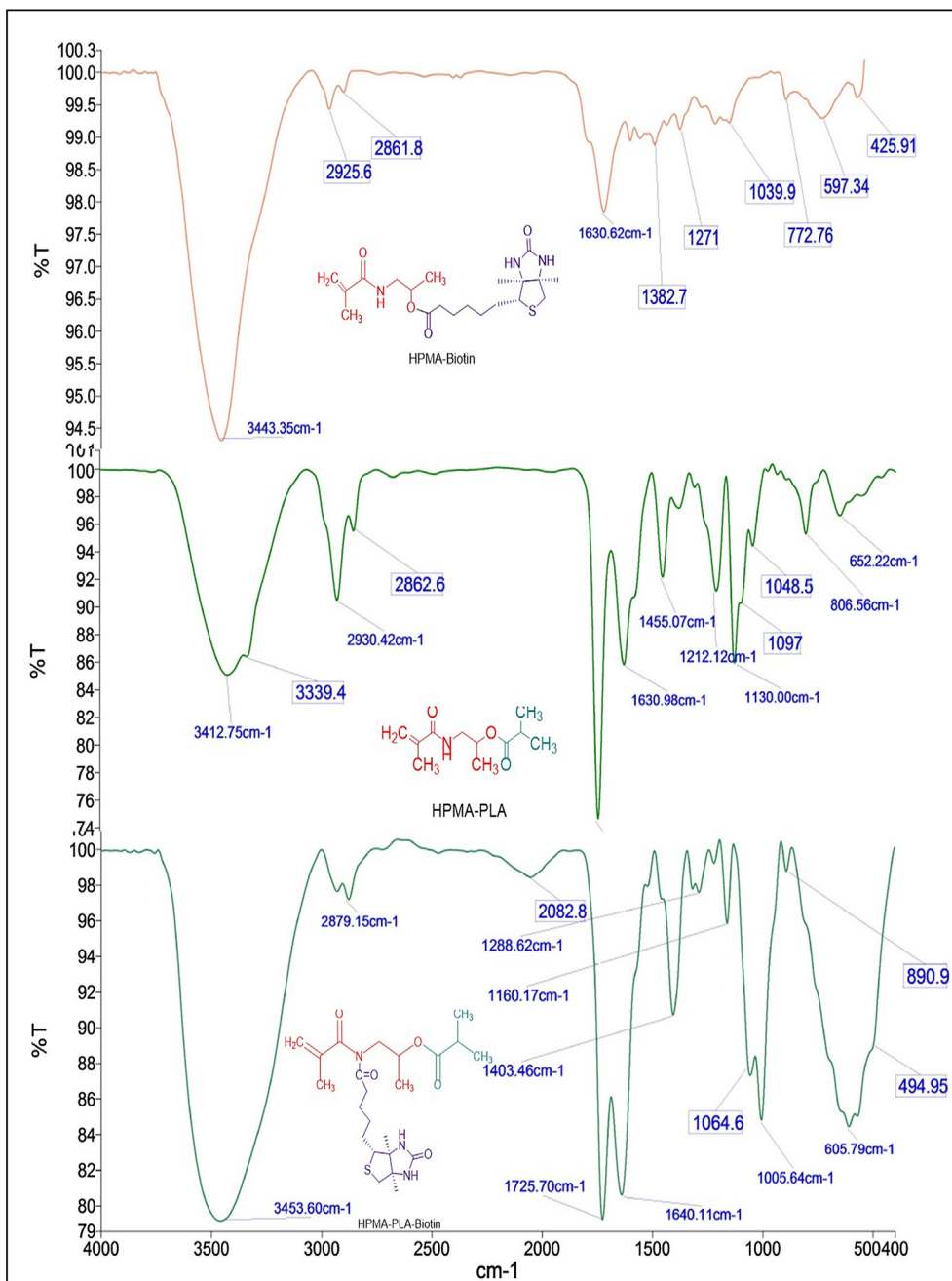


Fig. 2. FT-IR spectrum of prepared conjugates: HPBT, HPLA, and HPLA-BT. The samples were prepared through KBr pellet method.

used for fabrication of BTZ loaded PNPs. Following the o/w single emulsion method (Prabu et al., 2009), weighed co-polymeric conjugates (10 mg) were dissolved in 5 mL of DCM separately. Then, 0.1% w/v PVA solution was dissolved in distilled water and added to the copolymeric solution. BTZ dissolved in methanol and lecithin solution (4% ethanol and heated at 65 °C) were added dropwise (1 mL/10 min) with stirring. The reaction vessel was left stirred to evaporate the organic solvent. At the last, the nanoparticles were vortexed for 5–7 min and was dialyzed using dialysis membrane (MWCO 10 kDa) for the entire day. Finally, the PNPs solution was collected, lyophilized and stored at –20 °C for further studies (Rosca et al., 2004). In total, the three blank PNPs i.e. HPBT, HPLA, HPLA-BT and three BTZ loaded (or drug loaded) PNPs i.e. DL-HPBT, DL-HPLA, DL-HPLA-BT were prepared successfully.

#### 2.4. Characterization of HPLA-BT PNPs

##### 2.4.1. <sup>1</sup>H NMR spectroscopy

<sup>1</sup>H NMR spectra were recorded to discriminate the blank and drug loaded PNPs Fig. S5. All the samples were dissolved in D<sub>2</sub>O (deuterated) solvent and processed in 500 MHz NMR spectrometer (Bruker Ascend 500 MHz spectroscopy, Switzerland).

##### 2.4.2. Particle size, zeta potential, PDI (polydispersity index)

The prepared PNPs were characterized by zeta sizer Nano ZS (Malvern Instruments, Malvern, UK) for particle size, zeta potential and PDI. Zeta sizer is based on the principle of photon correlation spectroscopy (PCS) where the average particle size was calculated by measuring the wideness of particle size distribution. The PNPs were suspended in 1 mL deionized water and filtered the solutions by syringe filter (0.22 μm) before measurement. Results were expressed as triplet

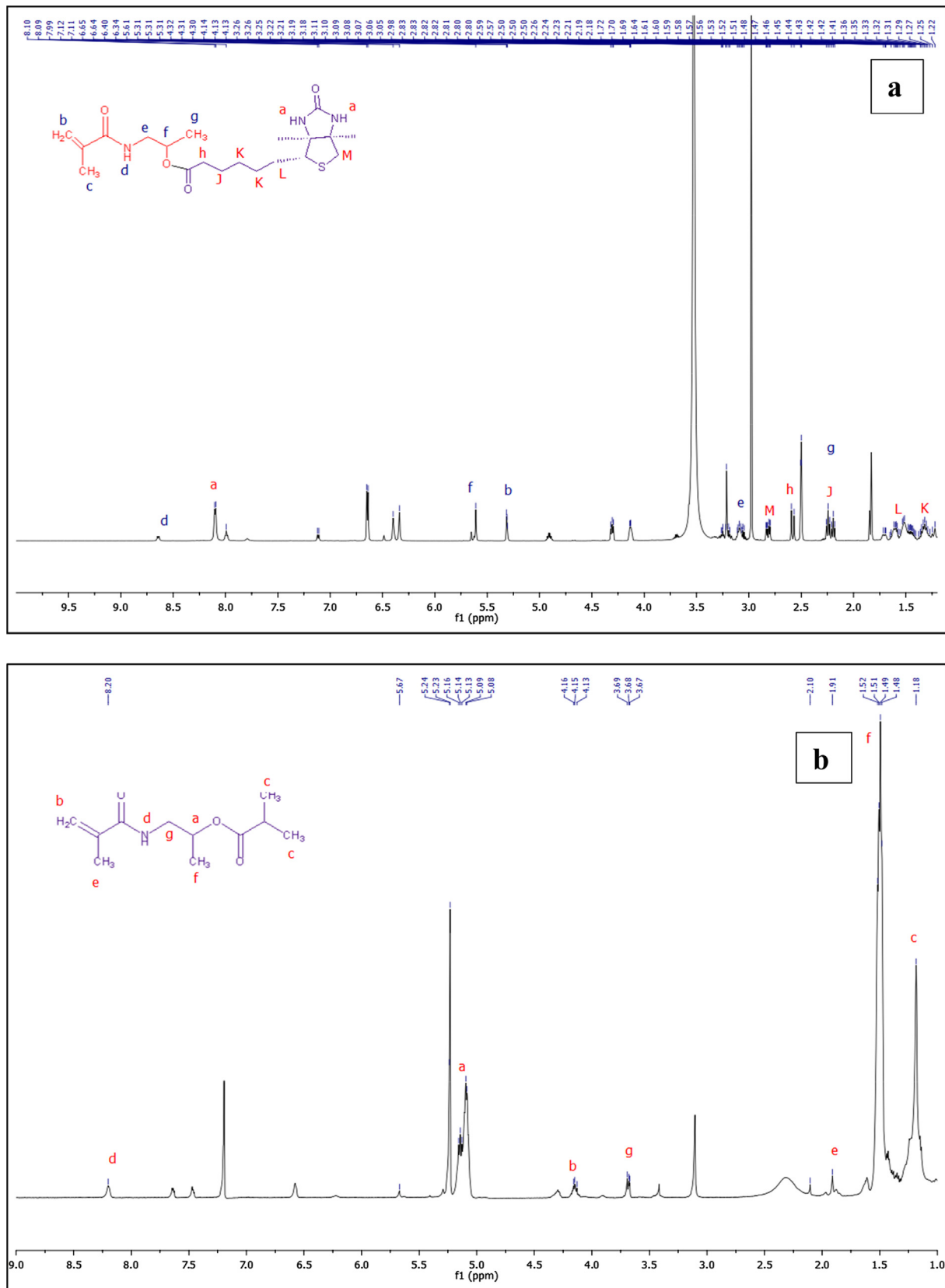


Fig. 3.  $^1\text{H}$  NMR spectrum of (a) HPBT (b) HPLA and (c) HPLA-BT. Deuterated solvents were used for the preparation of sample for NMR analysis.

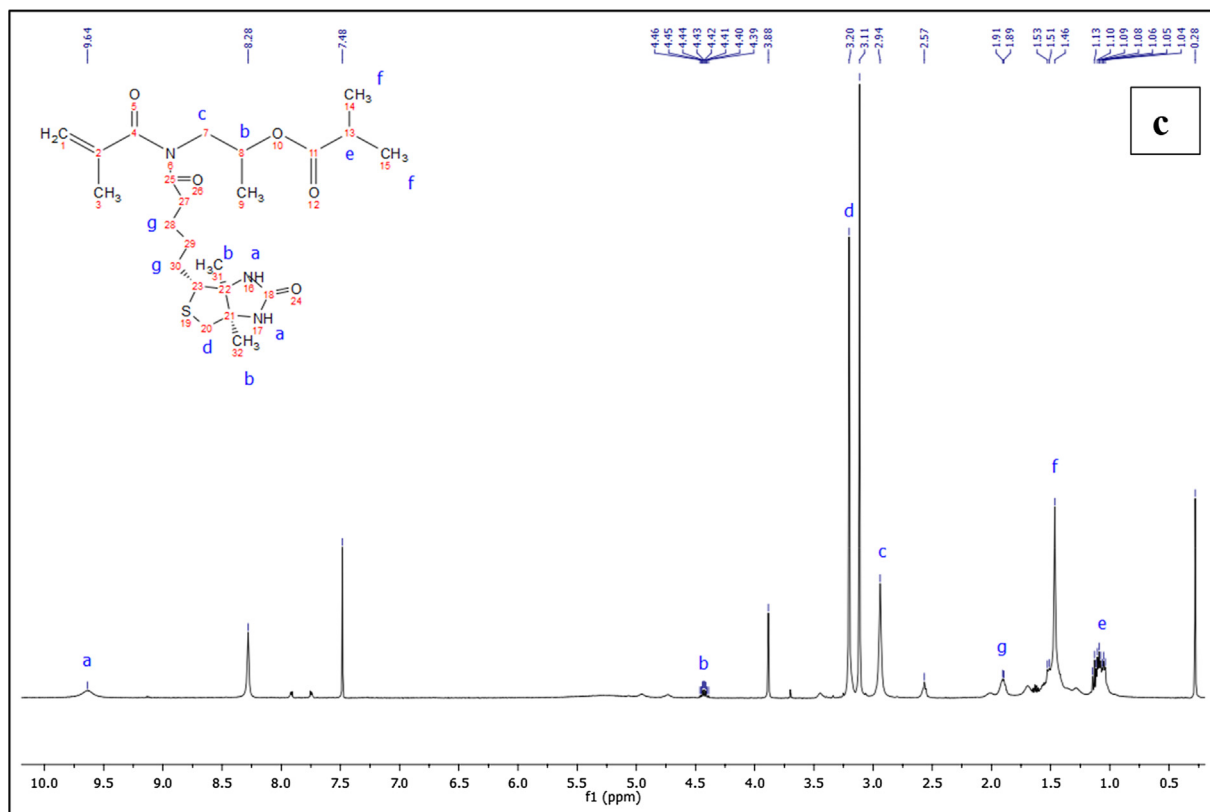


Fig. 3. (continued)

Table 1

Particle size, zeta potential, drug loading capacity (% DLC) and drug entrapment efficiency (% DEE) of the prepared formulations.

Formulation Code	Size (nm)	Zeta potential (mV)	PDI	Entrapment efficiency (% DEE)	Drug loading (% DLC)
HPBT PNPs	213.6 ± 0.25	-7.64 ± 1.23	0.150 ± 3.02	-	-
DL-HPBT PNPs	279.7 ± 2.21	-1.07 ± 1.28	0.131 ± 0.22	83.59 ± 0.05	14.75 ± 0.13
HPLA PNPs	356.3 ± 2.21	-2.47 ± 0.56	0.254 ± 0.24	-	-
DL-HPLA PNPs	430.5 ± 2.21	-17.78 ± 0.12	0.269 ± 0.13	74.68 ± 0.08	17.93 ± 0.12
HPLA-BT PNP	185.3 ± 0.21	-6.50 ± 1.12	0.287 ± 0.02	-	-
DL-HPLA-BT PNPs	199.7 ± 1.32	-3.20 ± 0.22	0.196 ± 0.11	82.20 ± 0.14	19.73 ± 0.03

of mean ± SD (Table 1).

#### 2.4.3. Surface morphology (atomic force microscopy; AFM)

Microscopy was performed using AFM for evaluating surface characteristics (Fig. 4). For AFM analysis, fresh samples were prepared by dispersion of PNPs in double distilled water. The dried thin film of samples was spread over the silicon wafer using spin coating phenomenon. Silicon wafer were dried, and excess of water was drawn off using filter paper. The results were recorded using Bruker nanoscope V software and images were taken with 256 × 256-pixel camera, and 300 Hz cantilever frequency after measuring the various sections of thin film samples. Ra (average roughness value) and Rq (root mean square roughness defined the surface texture and kurtosis value told about the bumpy, spiky and perfectly random surface (Kumar and Rao, 2012).

#### 2.5. Drug loading capacity (DLC) and drug entrapment efficiency (DEE)

The drug loading capacity of prepared PNPs (i.e. DL-HPBT, DL-HPLA, and DL-HPLA-BT) was determined by membrane dialysis method

(Table 1). Nanoparticles suspension (2 mL) was filled in dialysis bag (MWCO 5 kDa, Hi-media Laboratories Pvt. Ltd., Bangalore, India) and dialyzed against perfect sink conditions for 2 h to allow the untrapped drug drawn off from the dialysis bag. The amount of untrapped drug was analyzed at 270 nm using HPLC. The % DEE and % DLC was calculated using the mentioned equations.

$$\%DEE = \frac{\text{Total drug feed} - \text{Amount of untrapped drug}}{\text{Total drug feed}} \times 100$$

$$\%DLC = \frac{\text{Total drug feed} - \text{Amount of untrapped drug}}{\text{Total polymer feed}} \times 100$$

#### 2.5.1. HPLC (High performance liquid chromatography)

BTZ estimation during release and other biological studies was performed using reverse phase HPLC analysis. The reverse phase HPLC (RP-HPLC) analysis was performed at Central University of Rajasthan, Ajmer. The HPLC system used was Shimadzu LC-2010 CHT (Tokyo, Japan) with PDA detector. Merck HPLC column (RP C<sub>18</sub>,

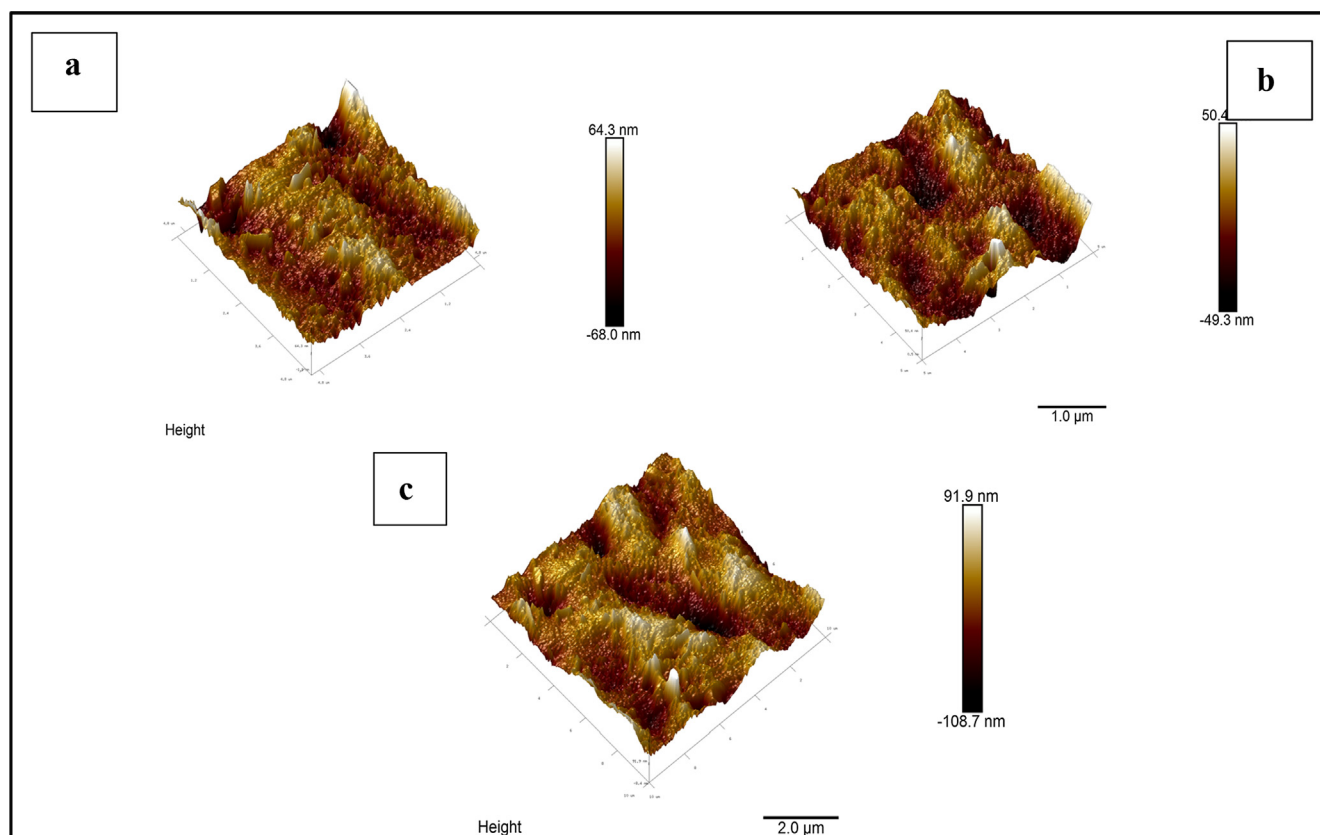


Fig. 4. Atomic force microscopy (AFM) of DL-HPLA-BT PNPs. The scale bar of 1.0  $\mu\text{m}$  in image (a) and (b) and 2.0  $\mu\text{m}$  in image (c) represented.

4.6 mm  $\times$  250 mm) was used throughout the analysis. The mobile phase utilized consisted of HPLC grade acetonitrile (ACN), water and formic acid (HCOOH) in 70:30:0.1% v/v, respectively. The flow rate and temperature were maintained to be 1.0 mL/min and 25  $^{\circ}\text{C}$ , respectively. The area under curve of the samples was analyzed at 270 nm (Byrn et al., 2011; Kamalzadeh et al., 2017).

## 2.6. *In vitro* release and kinetic models

Time dependent release of BTZ from prepared polymeric nanoparticles was performed in buffer solutions pH 7.4 and 5.6 mimicking the physiological conditions of blood and endosomes, respectively (Gupta et al., 2018). Briefly, 2 mL suspension of the developed nanoformulation was filled in a dialysis bag (MWCO 5 kDa, Hi-Media Laboratories Pvt. Ltd., Bangalore, India) and immersed in 100 mL of PBS (pH 7.4) under stirred condition (150  $\pm$  40) rpm. Two milliliters of aliquots were withdrawn at defined time intervals and the same amount of PBS was replenished in to the beaker to maintain sink conditions throughout the release study protocol. Similar protocol was followed to obtain the *in vitro* release data at pH 5.6 using buffer solution as release media. The drug released from formulations was estimated using HPLC method as mentioned earlier. Further, kinetic models were applied for the prepared formulations to recognize the best fitted kinetic model among different non-linear kinetic models such as, zero order, first order, Higuchi, Korsmeyer-Peppas and Hixson Crowell model.

## 2.7. Hemolytic toxicity study

The hemolytic toxicity study of BTZ, DL-HPBT PNPs, DL-HPLA PNPs, and DL-HPLA-BT PNPs was performed in concentration dependent manner (Codony-Servat et al., 2006). The whole blood was collected from a healthy volunteer and stabilized by EDTA. The plasma was removed after centrifugation at 1250 rpm (R-4C DX, REMI, India)

for 10–15 min. The collected RBCs were washed twice using normal saline (0.9% w/v) and finally, diluted in 1:10 ratio with normal saline. RBCs suspension (0.8 mL) was mixed with 3.2 mL of the test solutions to make the final concentration 10, 50, 100 and 150  $\mu\text{g}/\text{mL}$ . Distilled water and normal saline were regarded as the positive and negative control, respectively. The cell suspension were incubated for 2 h, and centrifuged. The extracted supernatant was analyzed at 540 nm using UV-visible double spectrophotometer (Perkin Elmer). The percentage hemolysis was calculated using the following equation.

%Hemolysis

$$= \frac{\text{Absorbance of test} - \text{Absorbance of negative control}}{\text{Absorbance of positive control} - \text{Absorbance of negative control}} \times 100$$

## 2.8. Cytotoxicity study

The cytotoxicity of BTZ, DL-HPBT PNPs, DL-HPLA PNPs, and DL-HPLA-BT PNPs was evaluated by MTT assay against MCF-7 breast cancer cell line (Yang et al., 2009). The cell lines were grown in culture media DMEM (Dulbecco's Modified Eagle's Medium) containing 10% v/v FBS (Fetal bovine serum) and 1% v/v L-Glutamine-Penicillin-Streptomycin solution. The cells were seeded uniformly at a density of  $1 \times 10^4$  cells per well into 96-well plates and incubated overnight in  $\text{CO}_2$  incubator (Hera cell 150i, Thermo Fisher). After 90% confluency, the cells were treated with different concentration range of formulations and incubated for 24 h (complete media alone was used as control). Next day, the cells were removed and washed thrice with PBS and to each well 50  $\mu\text{L}$  of MTT solution was added and left for another 4 h incubation. Later, 150  $\mu\text{L}$  dimethyl sulfoxide (DMSO, HPLC grade) was mixed into each well to dissolve the formazan crystals and a violet color appeared in each well. The absorbance was taken at 570 nm using ELISA plate reader (Omega Fluostar) after incubation for 10 min. The

IC<sub>50</sub> values were determined using Microsoft Excel.

### 2.9. Cellular uptake study

In order to investigate the cell uptake potential of prepared formulations, cellular uptake study was performed utilizing fluorescein isothiocyanate (FITC) labeling of MCF-7 cells (Doerflinger et al., 2018). The prepared formulations were labelled with FITC (2 mg/mL) via FITC tagging reaction to examine the cell uptake by different drug loaded PNPs formulations (i.e. DL-HPBT PNPs, DL-HPLA PNPs, and DL-HPLA-BT PNPs). Briefly, 2.5 mg of FITC was dissolved in 1 mL of acetone. Then, in a 25 mL RBF, 1 mL PBS of pH 7.4 were mixed with FITC solution and stirred. After 30 min, drug loaded formulations were added. The reaction was carried out in dark conditions for 24 h. For study purpose, MCF-7 cells ( $4 \times 10^3$  cells per well) were seeded in a 6-well plate and incubated overnight. Next day, the culture media was removed from each well and then the cells were treated with FITC (2 mg/mL) tagged formulations diluted with culture media into each well for predetermined time interval of 2, 4 and 24 h. FITC treated cells were considered as control for this experiment. The images were captured under OLYMPUS CKXF3 fluorescence microscope using 10 and 40x magnifications.

### 2.10. In vivo pharmacokinetic study

All the animal experimentations performed were approved by the Institutional Animal Ethical Committee, Rungta College of Pharmaceutical Sciences and Research, Bhilai, India. *In vivo* pharmacokinetic studies were performed on healthy unisex Sprague Dawley rats weighing 250–300 gm (Nie et al., 2017). All the animals were kept on standard diet and water throughout the experiment. The animals were divided into four groups, in which each group was comprised of 4 animals. The different group of animals were administered intravenously with BTZ, DL-HPBT PNPs, DL-HPLA PNPs, and DL-HPLA-BT PNPs in 1 mg/kg equivalent dose of BTZ in saline. At defined time intervals, 0.2 mL of blood sample was withdrawn from the retro orbital plexus and collected in a heparinized (anti-coagulant) vial. The supernatant was withdrawn after centrifugation of the sample withdrawn at 3000 rpm (R-4C DX, REMI, India). In each sample, 0.5 mL of acetonitrile was added and centrifuged immediately to denature blood proteins for better analysis. The concentration of the supernatant was then evaluated at 270 nm by reverse phase HPLC (Shimadzu LC-2010C, Japan) methods as explained in earlier paragraphs. The plasma concentration–time graph was plotted using the obtained data and various pharmacokinetic parameters were calculated following one compartment open body model (1 CBM) for *iv* push.

## 3. Results and discussion

### 3.1. Synthesis and characterization

#### 3.1.1. HPMA (N-2-hydroxypropylmethacrylamide)

HPMA co-polymer was synthesized following a previously reported protocol (Chytil et al., 2010). The white crystalline product with percent yield of 82% was confirmed for the synthesis through different spectroscopic techniques. The FT-IR spectrum revealed peaks at  $1653 \text{ cm}^{-1}$  for CONH,  $\text{CH}_3$  (methyl), and  $\text{CH}_2$  (methylene) peaks were seen at  $3299.74$ , and  $2974.29 \text{ cm}^{-1}$ , respectively (Fig. S1). The chemical shift at 7.7 ppm (s, CONH), OH peak at 5.3 ppm,  $\text{CH}_3$  peak at 1.2 ppm (t,  $-\text{CH}_3$ ), that further confirmed the synthesis of this co-polymer (Fig. S1).

#### 3.1.2. HPMA-Biotin (HP-BT)

HPMA was further conjugated to biotin (BT) (Fig. S2) via DCC/DMAP coupling reaction as shown in synthetic scheme (Fig. 1). In the FT-IR spectrum, peaks were seen at  $3443.35$  ( $-\text{CONH}$ ),  $2861.8$  (alkane),

$2925.6$  (alkene), and  $1630.62 \text{ cm}^{-1}$  ( $-\text{NH}$ ), which indirectly confirmed synthesis. Peaks at  $1271.1$  and  $1039.9 \text{ cm}^{-1}$  were of the chemically conjugated moiety ester, which confirmed the conjugation (Fig. 2). In the  $^1\text{H}$  NMR spectra,  $\delta$  ppm: 8.14 [ $-\text{NH}$ , HPMA(d)], 3.09 [t,  $-\text{CH}$ , HPMA (e)], 5.23 [s  $-\text{CH}_2$  (b)], 2.21 [m  $-\text{CH}$  (H)], 1.23 [m  $-\text{CH}$  (K)], and 2.74 [ $-\text{CH}_2$  (M)] were observed (Fig. 3(a)). Further confirmation was ensured by  $^{13}\text{C}$  NMR (500 MHz,  $\text{CDCl}_3$ )  $\delta$  ppm: 69.98 [CO (M)], 46.1 [C-N (N)], 172.0 [CO (P)], 140 [C (R)], 168.5 [OCO, HPBT], 22.5 [ $\text{CH}_2$  (K)], 41.0 [ $\text{CH}_2$  (e)], 161.85 [CO (C)], and 29.0 [ $\text{CH}_2$  (I)] (Fig. S5(a)).

#### 3.1.3. HPLA (HPMA-PLA conjugate)

HPMA-PLA conjugation was confirmed by;  $^1\text{H}$  NMR (500 MHz,  $\text{CDCl}_3$ )  $\delta$  ppm: 5.13 [m, CH, PLA (a)], 3.61 [ $\text{CH}_2$  (g)] 1.10 [s- $\text{CH}_3$  PLA (c)], 1.50 [t- $\text{CH}_3$  PLA (f)], 8.26 [s-NH (d)], and 1.92 [s- $\text{CH}_3$  (e)] (Fig. 3 (b)).  $^{13}\text{C}$  NMR (500 MHz,  $\text{CDCl}_3$ )  $\delta$  ppm: 169.3 [OCO, PLA (a)], 69.0 [CH, PLA (e)], 16.6 [ $\text{CH}_3$ , PLA(b)], 30.0 [s- $\text{CH}_3$  (d)], and 52.5 [ $\text{CH}_2$  (c)] (Fig. S5(b)). Likewise, the FT-IR peaks at  $1630.98$  (alkene),  $3339.4$  ( $1^\circ$  NH),  $2930.42$  ( $=\text{CH}$ ; alkene), and  $1720 \text{ cm}^{-1}$  (ester) wavenumbers confirmed peak for conjugation of HPMA and PLA (Fig. 2). Before conjugation the identity of the procured PLA was also confirmed through NMR spectroscopy (Fig. S3).

#### 3.1.4. HPLA-BT (HPMA-PLA-biotin)

The conjugation was ensured by  $^1\text{H}$  and  $^{13}\text{C}$  NMR spectroscopy at each step.  $^1\text{H}$  NMR (500 MHz, DMSO)  $\delta$  ppm: 9.64 [ $-\text{NH}$ , BT (a)], 4.43 [m  $-\text{CH}$  (b)], 1.13 [m  $-\text{CH}$  (e)], 1.53 [s  $\text{CH}_3$  (f)], 3.26 [d CH (d)], and 2.94 [ $\text{CH}_2$  (c)] (Fig. 3(c)).  $^{13}\text{C}$  NMR  $\delta$  ppm: 162.99 [OCO (a)], 22.99 [ $\text{CH}_3$  (b)], 14.13 [ $\text{CH}_3$  (c)], 23.34 [ $\text{CH}_2$  (d)], 53.32 [ $\text{CH}_2$  (e)], and 77.85 [m CH (f)]. FT-IR spectrum peaks at  $3453.60$  (CONH),  $1640.11$  ( $1^\circ$  NH; biotin),  $605.79$  ( $=\text{C-H}$ ),  $1725.70$  and  $1005.64 \text{ cm}^{-1}$  (ester peak) suggested the conjugation of HPLA with biotin (Fig. S5(c)). The intermediate biotin chloride (BT-Cl) was also characterized spectroscopically by  $^1\text{H}$  and  $^{13}\text{C}$  NMR analysis to confirm synthesis (Fig. S4). All the obtained spectral data favored the synthesis of polymeric conjugates.

#### 3.1.5. UV visible spectroscopic characterization of conjugates

UV Visible spectrophotometry was performed for drug as well as all the conjugates (Fig. S6). The peaks were clearly visible for biotin around 350 nm. This characterization step further supported the synthesis of HPBT and HPLA-BT.

## 3.2. Characterization of PNPs

Polymeric nanoparticles (PNPs) were prepared by o/w single emulsion method particularly to control or optimize the size and drug efficiency of nano-formulations. Finally, the three different formulations i.e. BTZ loaded HPLA PNPs (DL-HPLA), BTZ loaded HPLA-BT PNPs (DL-HPLA-BT), and BTZ loaded HPBT PNPs (DL-HPBT) were prepared, characterized, and evaluated in further steps for different outcomes and anticancer activities.

#### 3.2.1. Drug loading capacity (DLC) and drug entrapment efficiency (DEE)

The DLC of DL-HPLA-BT PNPs, DL-HPLA-PNPs and DL-HPBT was found to be  $19.73 \pm 0.03$ ,  $17.93 \pm 0.12$ , and  $14.75 \pm 0.13\%$ , respectively. DEE of DL-HPLA-BT, DL-HPLA and DL-HPBT PNPs was calculated to be  $82.20 \pm 0.14$ ,  $74.68 \pm 0.08$ , and  $83.59 \pm 0.05\%$ , respectively. A slight increase in the DLC was seen in DL-HPLA-BT PNPs as compared to DL-HPLA-PNPs. In the similar way, DEE of DL-HPLA-BT PNPs was higher than HPLA-PNPs (Table 1). The observed slight increase in the encapsulation can be seen probably due to surface engineering of the HPLA conjugates with biotin (BT) which might be providing more room for encapsulation within respective PNPs.

#### 3.2.2. UV-Visible spectroscopy

Maximum absorption is shifted towards longer wavelength (Fig. S6)

in case of DL-HPLA-BT PNPs due to the presence of carbonyl bond in the polymeric conjugate. BTZ absorption can be observed at 300 and 310 nm wavelengths. However, the blank polymeric conjugates showed a less intensified absorption and the overlapped wavelengths were not able to detail any clear indication. The maximum absorption of DL-HPLA-BT PNPs was an indication of conjugation of HPLA with BT forming a carbonyl bond elucidated as characteristic peak in UV-visible graph.

### 3.2.3. $^1\text{H}$ NMR analysis for BTZ loaded formulations

The  $^1\text{H}$  NMR spectra (Fig. S8) showed a difference between PNPs (blank polymeric nanoparticles) and drug loaded-PNPs (DL-PNPs). A sharp peak was noticed at a chemical shift of 3.31 ppm in DL-HPLA-BT PNPs, which is due to the hydrogen atoms attached to the carbon group near to boron atom in BTZ structure while this peak was absent in B-HPLA-BT PNPs. These results indicated the encapsulation of BTZ in DL-HPLA PNPs.

### 3.2.4. Particle size, zeta potential, PDI (polydispersity index), and microscopy

The followed strategy yielded mean particle sizes of formulations such as DL (drug loaded or BTZ loaded)-HPLA-BT PNPs, HPLA-BT PNPs, DL-HPLA PNPs, HPLA PNPs, DL-HPBT PNPs and HPBT PNPs  $199.7 \pm 1.32$ ,  $185.3 \pm 0.21$ ,  $430.5 \pm 2.21$ ,  $356.3 \pm 2.21$ ,  $279.7 \pm 2.21$ , and  $213.6 \pm 0.25$  nm, respectively in a narrow size range (Table 1). The size can have major impact in drug targeting to tumors as the tumor vasculature cut-off size band varies from 100 to 800 nm (Ren et al., 2015). So, the size of the nanocarriers can be controlled to deliver through the efficacious EPR-mediated approach. The results obtained for particle size suggested that the DL-HPLA-BT PNPs size lies in 200 nm range that may be helpful for tumor targeting (Torchilin, 2011). The small size particles can enter in the tumor cells effortlessly and can produce drug action with a great extent. The size, zeta potential, PDI, % DLC, and % DEE of formulation were tabulated in (Table 1). The prepared PNPs exhibited negative zeta potential which might be due to the presence of ester groups in HPBT, HPLA and HPLA-BT.

### 3.2.5. Surface morphology evaluation by atomic force microscopy (AFM)

The surface morphology of PNPs was observed by atomic force microscopy (AFM). AFM was performed only for DL-HPLA-BT PNPs which described the surface topography and texture of these PNPs. The surface roughness (Ra) 27.2 nm, root mean square roughness (Rq) 20.2, and skewness 0.168 were observed during analysis. The high kurtosis value of 4.37 has given the idea of spiky surface or high-pitched peak surface for DL-HPLA-BT PNPs (Singh et al., 2019). The overall AFM results concluded that the PNPs showed surface roughness with heightened peaks (Fig. 4).

### 3.3. In vitro release and kinetic models

Drug release profile is the key determinant factor to know about the therapeutic performance of a drug in delivery system. At pH 7.4, approx. 55% and approx. 34% of BTZ was released from DL-HP-BT PNPs and DL-HPLA-BT PNPs, respectively in 4 h (Fig. 5a). Similarly, greater than 80% of BTZ was released from DL-HP-BT PNPs, and approx. 76% drug was released from DL-HPLA PNPs while DL-HPLA-BT PNPs released more than 65% of BTZ in 24 h of time point. These results suggested that DL-HPLA-BT PNPs owed slow and controlled release pattern than DL-HP-BT PNPs and DL-HPLA PNPs. The controlled release of drug could be beneficial to maintain an appropriate drug concentration in the tumor cells for a prolong period of time so as to improve the overall drug action. These results gave an idea that the drug was encapsulated in the hydrophobic core of nanoparticles and showed a controlled released slowly at pH 7.4 (Fig. 5a). At pH 5.6 (Fig. 5b) greater than 50% of BTZ was released from DL-HP-BT PNPs

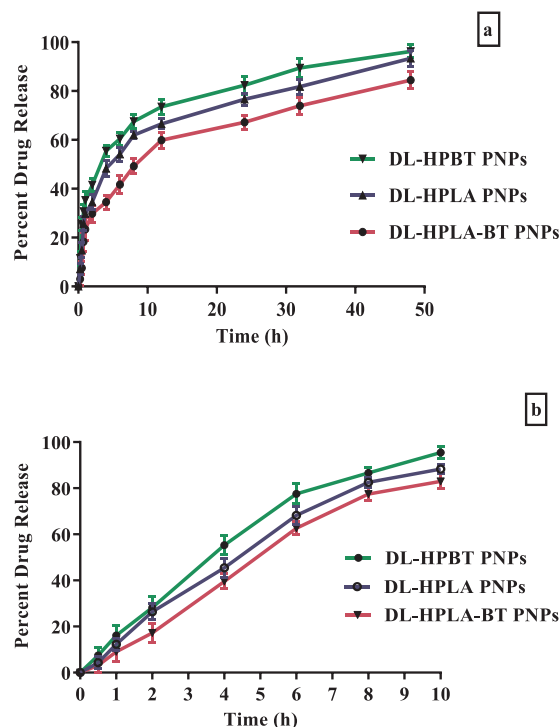


Fig. 5. *In-vitro* drug release pattern of BTZ, DL-HPBT PNPs, DL-HPLA PNPs and DL-HPLA-BT PNPs at pH (a) 7.4 (b) 5.6. Membrane dialysis method was followed for the release studies *in vitro*.

and approx. 45% DL-HPLA PNPs, while it was less than 40% for DL-HPLA-BT PNPs in 4 h. More than 80% drug was released from DL-HPLA-BT PNPs in 10 h. Conclusively, faster drug release was noticed at pH 5.6 for the DL-HPLA-BT PNPs than at physiological pH. The pH 5.6 may be favorable for inducing significant anti-cancer effect of BTZ as tumorous environment is acidic in nature. Different kinetic equations were tested to get a better fit kinetic model in the prepared formulations at pH 7.4 and 5.6. The results were tabulated in Table S1(a) and (b), respectively. Incorporating the obtained release data into the mentioned kinetic model, the best fit models at pH 7.4 for DL-HPLA-BT PNPs was found to be Korsmeier-Peppas model ( $R^2 = 0.98$ ), Higuchi model ( $R^2 = 0.95$ ) and first-order model ( $R^2 = 0.93$ ). In case of DL-HPLA PNPs, first-order model ( $R^2 = 0.92$ ), Higuchi model ( $R^2 = 0.94$ ), Korsmeier-Peppas model ( $R^2 = 0.90$ ) and for DL-HPBT PNPs, first-order model ( $R^2 = 0.93$ ), Higuchi model ( $R^2 = 0.91$ ), Korsmeier-Peppas model ( $R^2 = 0.90$ ) were the best fit models. At pH 5.6 the best fit models for DL-HPLA-BT PNPs were seen to be Higuchi model ( $R^2 = 0.91$ ), first-order model ( $R^2 = 0.90$ ), Korsmeier-Peppas model (0.94) and zero-order model ( $R^2 = 0.92$ ). For DL-HPLA PNPs the observations were Higuchi model ( $R^2 = 0.94$ ), first-order model ( $R^2 = 0.92$ ), Korsmeier-Peppas model (0.91), and zero-order model ( $R^2 = 0.96$ ). For DL-HPBT PNPs the observations were Higuchi model ( $R^2 = 0.95$ ), first-order model ( $R^2 = 0.96$ ), Korsmeier-Peppas model (0.94), and zero-order model ( $R^2 = 0.98$ ).

### 3.4. Ex-vivo hemolytic toxicity study

Concentration dependent hemolysis toxicity analysis (Fig. 6) was performed to determine the interaction of erythrocytes with BTZ and prepared formulations. BTZ displayed 24% hemolysis, whereas, DL-HPLA-BT PNPs showed only 12% hemolysis against RBCs at a concentration of 150  $\mu\text{g}/\text{mL}$  indicated that DL-HPLA-BT PNPs were 2-fold less toxic than BTZ with  $p < 0.0001$ . Interestingly, the biotin anchored HPLA-PNPs (i.e. DL-HPLA-BT PNPs) showed less toxicity probably due to biocompatible interaction of nanoparticles with erythrocytes. In

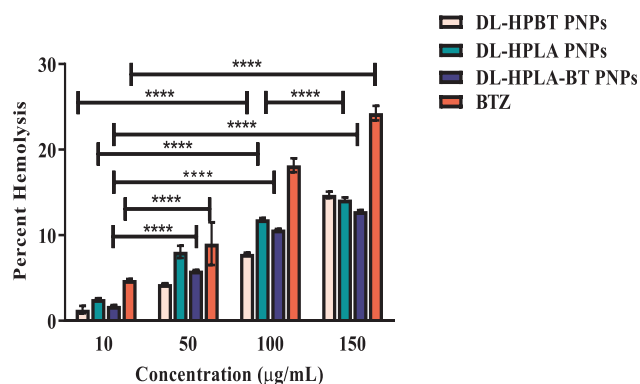


Fig. 6. *Ex vivo* hemolysis of BTZ and drug loaded (DL) PNPs of HPBT, HPLA, and HPLA-BT at different concentrations (10, 50, 100, and 150 µg/mL); Values represents mean  $\pm$  SD (n = 3). \*\*\*\* p < 0.0001 indicates the extremely significant difference between various concentrations of drug and drug loaded formulations (Two-way ANOVA; Bonferroni multiple comparisons test).

comparison to DL-HPLA-PNPs, the DL-HPBT PNPs exerted a minimal hemolytic toxicity on erythrocytes at similar concentration. At lower concentration of 10 µg/mL, a considerable decrease in hemolytic toxicity was noticed for DL-HPLA-BT PNPs than BTZ. The hemolytic toxicity for PNPs was 2-fold less than BTZ at 50 µg/mL, similarly 2-fold decrease was seen in case DL-HPBT PNPs than DL-HPLA PNPs. Peripheral neuropathy and thrombocytopenia are considered as dose limiting toxic effects of BTZ as per literature (Chen et al., 2011). This is also one reason that the study was planned and conducted.

### 3.5. Cytotoxicity assay

Cytotoxicity of drug-loaded formulations was examined against

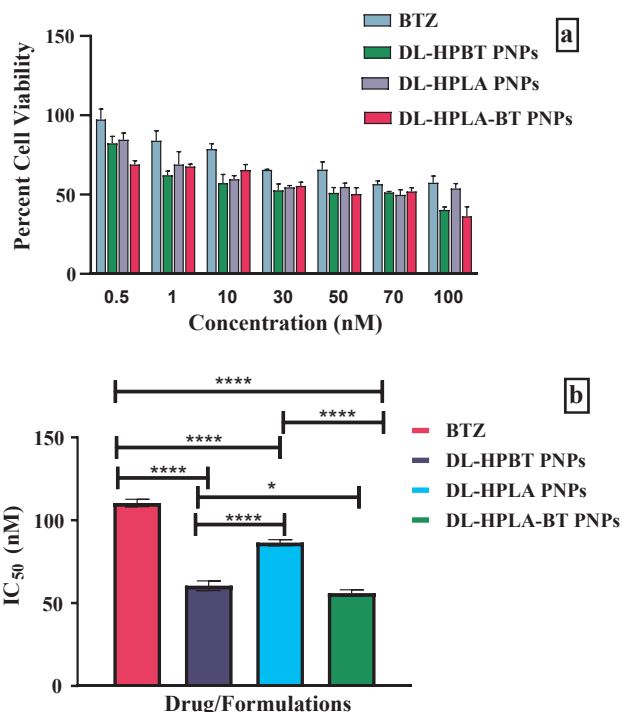


Fig. 7. (a) Percent cell viability of BTZ and DL-HPBT PNPs, DL-HPLA PNPs, and DL-HPLA-BT PNPs. The data obtained was part of the MTT assay performed at different concentrations. (b)  $IC_{50}$  of BTZ and DL-HPBT PNPs, DL-HPLA PNPs, and DL-HPLA-BT PNPs. \*\*\*\* indicates the extremely significant difference with p < 0.0001, while \* indicates less significant difference with p < 0.05 (Newman-Keuls multiple comparison test).

MCF-7 breast cancer cell lines through MTT assay (Fig. 7a and Fig. S9a). BTZ showed variable cytotoxicity against breast cancer cell line MCF-7 ( $IC_{50}$  = 100  $\pm$  8.4 nM), MDA-MB-231 ( $IC_{50}$  = 7  $\pm$  2.7 nM), MDA-MB-468 ( $IC_{50}$  = 5  $\pm$  2.4 nM) and MDA-MB-453 ( $IC_{50}$  = 100  $\pm$  12.1 nM) (Doerflinger et al., 2018). The  $IC_{50}$  values calculated for DL-HPBT-PNPs was 56.06  $\pm$  0.12 nM, which was 1.97 (approx. 2-fold) less than BTZ with p < 0.0001 as per the experimental results while blank PNPs of HPLA-BT were found to be non-toxic to MCF-7 cells (Fig. S9B). Results inferred that significant reduction in  $IC_{50}$  values was observed for biotin conjugated PNPs (DL-HP-BT PNPs and DL-HPLA-BT PNPs). However, significant reduction in  $IC_{50}$  values was seen for DL-HPBT PNPs and DL-HPLA-BT PNPs as compare to DL-HPLA PNPs which indicates the role of biotin in ascertaining enhanced anticancer activity of biotin conjugated formulations against MCF-7 breast cancer cells. The biotinylated formulations acted efficiently than non-biotinylated one. The drug loaded PNPs (DL-HP-BT PNPs, DL-HPLA PNPs, and DL-HPLA-BT PNPs) exhibited higher cytotoxicity at lower concentration of drug as compared to pure BTZ against MCF-7 breast cancer cells (Fig. 7b). These results revealed that drug loaded PNPs possessed significant anti-cancer effect.

### 3.6. Cellular uptake study

The intracellular uptake of free BTZ and BTZ loaded formulations (DL-HPBT PNPs, DL-HPLA PNPs, and DL-HPLA-BT PNPs) was investigated by fluorescence microscopy using FITC (fluorescence isothiocyanate) dye. Here, we used biotin which acts as a cell targeting molecule and can be taken up by tumor cells selectively as per reported literature (Yang et al., 2009). Biotin receptors are overexpressed in cancerous cells and biotin can be used in tracking of tumor surface via prepared nanoparticles tagged with polymers as cargo (Vineberg et al., 2014). Therefore, now-a-days targeting ligand-based therapeutics has become a choice of drug targeting that can directly enter into tumor cells/surface. It was inferred that higher uptake of biotinylated PNPs than non-biotinylated HPLA-PNPs was seen in 2 h time (Fig. 8). This may be due to the targeting potential of biotin attached to HPLA-BT PNPs. Similarly, HPBT PNPs exhibited more uptake than HPLA PNPs (Fig. 8). Higher uptake of drug loaded PNPs was observed in the cells in a time dependent manner. This plausible effect ensured more surface binding affinity of biotin to tumor cells surface in case of HPLA-BT nanoparticles than non-biotinylated HPLA PNPs. Similarly, biotin conjugated HPMA PNPs (HPBT PNPs) showed more intensity than non-biotin conjugated HPLA-PNPs after 24 h. This may be due to the appropriate biotin tethering on the surface of HPLA-BT PNPs. From these findings, it was concluded that developed HPLA-BT PNPs could be used for effective breast cancer targeting using biotin as a ligand.

### 3.7. In vivo pharmacokinetic study

The BTZ calibration curve was prepared via RP-HPLC method optimized by ACN: Methanol: Water (70: 30: 0.1) as mobile phase to obtain a sharp peak of drug (Fig. S7) (Kamalzadeh et al., 2017). The positive and encouraging results obtained from *in vitro* release studies, cellular uptake, and cytotoxicity study impelled us for the *in vivo* pharmacokinetic studies in Sprague Dawley rats. Time dependent plasma drug concentration of BTZ, DL-HPBT PNPs, DL-HPLA PNPs, and DL-HPLA-BT PNPs were plotted in Fig. 9. The desired pharmacokinetic parameters were estimated by indicating the data into one compartmental open body (1 CBM) *i.v.* push model. The high elimination rate constant of drug and relatively low K values supports the intended objectives of the study. The elimination rate constant of DL-HPLA-BT PNPs was observed to be less than pure drug. The bioavailability ( $AUC_{0-\infty}$ ) of DL-HPLA-BT PNPs was enhanced by 8.5 folds than BTZ. A reduction in  $V_d$  was calculated for DL-HPBT PNPs (Table 2). The half-life of DL-HPLA-BT PNPs was increased by approximately 2.52 times than BTZ. The increase in bioavailability, half-life and decrease in

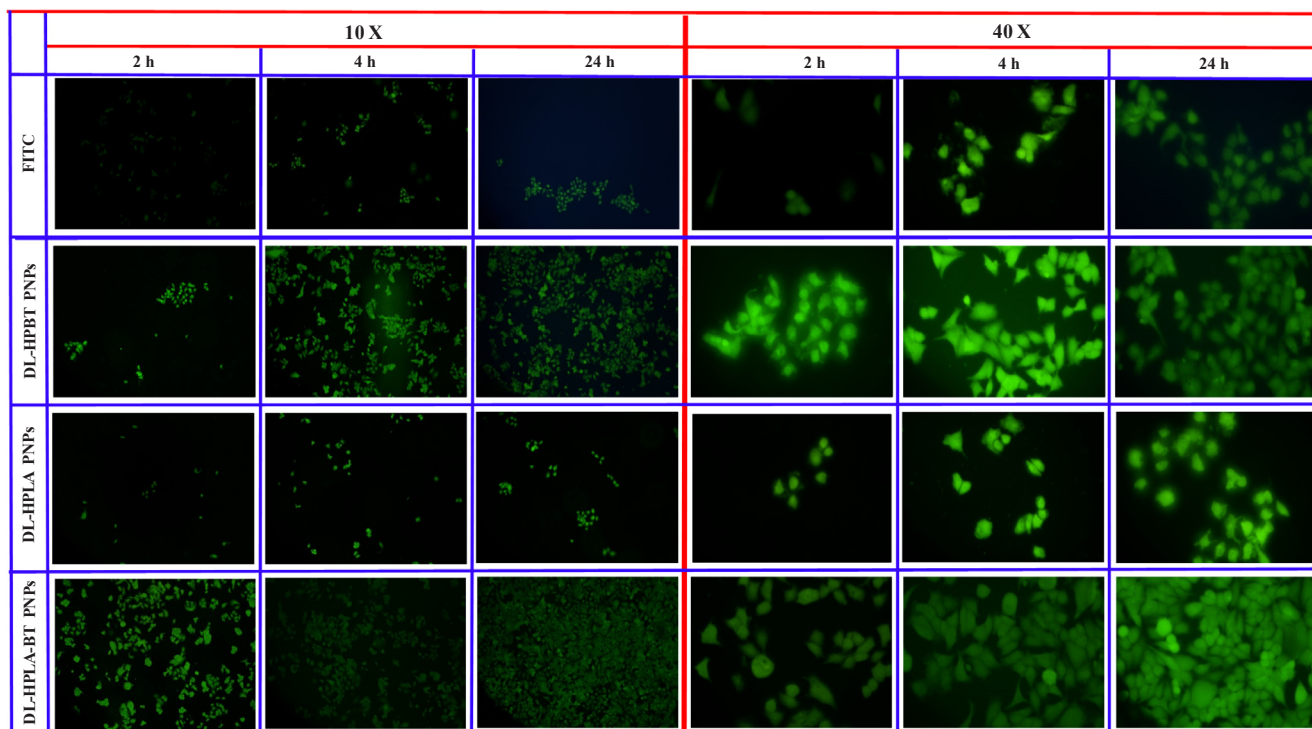


Fig. 8. Cellular uptake study of (a) FITC (fluorescein isothiocyanate) as control; (b) DL-HPBT PNP; (c) DL-HPLA PNP; (d) DL-HPLA-BT PNP performed against MCF-7, breast cancer cell line. FITC tagged formulations were used for the cellular uptake studies of drug loaded formulations.

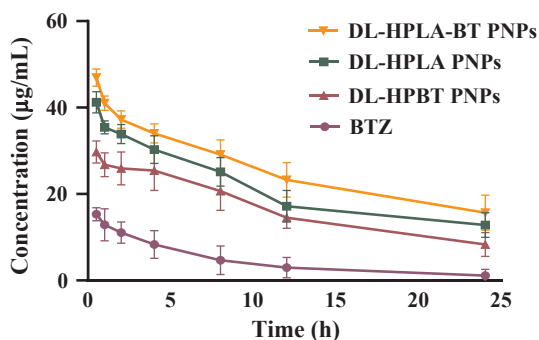


Fig. 9. Plasma concentration–time profile of DL-HPLA-BT PNP, DL-HPLA PNP, DL-HPBT PNP and BTZ obtained from *in vivo* pharmacokinetic study in Sprague-Dawley rats followed by intravenous administration of formulations with BTZ equivalent dose of 1 mg/mL. Values represents mean  $\pm$  SD (n = 4).

clearance rate confirmed the increment in the retention time of the formulations. Overall the pharmacokinetic study reflected the results obtained in *in vitro* release study. The higher retention time in terms of improved bioavailability is an indirect evidence of the sustained

behavior of DL-HPLA-BT PNP.

This study is a mix of polymeric synthesis exhaustively supported by the extensive characterization as well as the exploration of these developed conjugates for targeted delivery of BTZ. However, polymeric conjugation is a complex task to achieve, but present attempt was successful in synthesizing and characterizing polymeric conjugates through  $^1\text{H}$  NMR,  $^{13}\text{C}$  NMR, FT-IR and UV–visible spectroscopy. In the previous reports, HPMA based drug encapsulation and conjugation has been reported which did enter in the clinical trials too. The characteristics properties of HPMA enforces to utilize it for improving BTZ delivery in breast cancer cells. HPMA-PLA (HPLA) block copolymers were synthesized following the mechanism relied on an active ester and amide functionality approach. Then, the polymeric conjugates were fabricated into PNP by o/w emulsionsification. The obtained results can be clearly correlated with the effect of size and biotinylation. The cytotoxicity data is indicative to emphasize on significant aspects of HPMA over pure drug delivery. BTZ is relatively new molecule for establishing delivery strategy. In this regard the study can be significant contribution. The prepared PNP were able to demonstrate the influence of polymeric conjugation in the form of nanoparticles to investigate hemolytic toxicity, cytotoxicity, cellular uptake, and *in vivo*

Table 2

Pharmacokinetics Parameters of BTZ, DL-HPBT PNP, DL-HPLA PNP and DL-HPLA-BT PNP by Intravenous Administration in Sprague Dawley Rats. Values represent mean  $\pm$  S.D, AUC = area under the curve, K(h) elimination rate constant,  $t_{1/2}$  = plasma half-life, Cl = clearance, Vd = volume of distribution.

PK parameters	BTZ	DL-HPBT PNP	DL-HPLA PNP	DL-HPLA-BT PNP
AUC <sub>0-t</sub> ( $\mu\text{g mL}^{-1}\text{h}^{-1}$ )	102.74 $\pm$ 0.28	391.60 $\pm$ 0.022	493.21 $\pm$ 0.01	596.95 $\pm$ 0.15
AUC <sub>0-∞</sub> ( $\mu\text{g mL}^{-1}\text{h}^{-1}$ )	112.90 $\pm$ 0.32	546.27 $\pm$ 0.02	755.38 $\pm$ 0.021	955.51 $\pm$ 0.23
k ( $\text{h}^{-1}$ )	0.110 $\pm$ 0.01	0.054 $\pm$ 0.011	0.049 $\pm$ 0.001	0.044 $\pm$ 0.02
$t_{1/2}$ (h)	6.28 $\pm$ 0.04	12.91 $\pm$ 0.14	14.19 $\pm$ 0.011	15.84 $\pm$ 0.01
V <sub>d</sub> (L)	18.65 $\pm$ 0.024	8.40 $\pm$ 0.02	6.70 $\pm$ 0.24	5.90 $\pm$ 0.31
Cl (L/h)	2.058 $\pm$ 0.03	0.451 $\pm$ 0.12	0.33 $\pm$ 0.20	0.258 $\pm$ 0.03

pharmacokinetics. BTZ loaded HPLA-BT PNPs were also less hemolytic than the drug. It is also noticed in the previous literature that, BTZ exhibited hemolytic toxicity behavior as a side-effect of chemotherapy. The cell-line based study inferred that BTZ loaded PNPs were more cytotoxic than BTZ. From the cellular uptake studies, it was concluded that DL-HPLA-BT PNPs can enter into the MCF-7 breast cancer cells more efficiently than the pure drug. The enhanced cellular uptake may be due to the biotinylation of HPMA in HPMA-BT and HPMA-PLA-BT polymeric conjugates. Biotin overexpression on receptors in breast cancer cells may be one of the reasons why the uptake was enhanced in case of biotinylated PNPs in comparison to non-biotinylated one. Of course the better outcome can be evaluated only with the *in vivo* studies performed in breast cancer induced animal model, but we decided to carry out the *in vivo* studies first in normal healthy rats. The objective was to ensure, what kind of pharmacokinetic profile is displayed by the prepared PNPs. The obtained results were encouraging and supported the hypothesis that the prepared PNPs were able to exert the stealth nature as per as plasma drug concentration is concerned.

#### 4. Conclusions

Polymeric nanoparticles of BTZ were reported in the past but hitherto no one reported the biotin conjugated HPMA and PLA polymeric conjugates (HPLA-BT) and their modifications in to PNPs for BTZ delivery. In conclusion, HPMA co-polymer and its polymeric conjugates such as HPMA-Biotin/HP-BT, HPMA-PLA/HPLA, and HPMA-PLA-Biotin/HPLA-BT were successfully conjugated which are being reported for the first time for targeted delivery of BTZ. The research work includes synthesis of three polymeric conjugates as mentioned above. Particularly, the BTZ loaded HPMA-PLA-Biotin/HPLA-BT polymeric nanoparticles showed high drug loading capacity and encapsulation efficiency within 200 nm size range. BTZ loaded HPLA-BT PNPs represented an attractive and innovative approach to improve the efficacy of BTZ for breast cancer therapy in a targeted manner. The high drug loading capacity of PNPs have promising potential for BTZ against solid tumor. The prepared PNPs exhibited reduced hemolytic toxicity than BTZ in a concentration dependent study. The *in vitro* release studies suggested sustained and controlled release of drug at pH 7.4 however, faster drug release was observed at pH 5.6 (endosome). This suggested that the rate of release depends on variant pH conditions. The smart target moiety biotin successfully enhanced the internalization of BTZ loaded PNPs such as HP-BT and HPLA-BT thereby improving the anticancer activity of BTZ. The cytotoxicity study also indicated the higher cytotoxic effects of DL-HPLA-BT PNPs on MCF-7 cell lines. The decrease in IC<sub>50</sub> values for the prepared formulations supported the potential of biotin functionalized PNPs for breast cancer therapy. *In vivo* kinetics result revealed the increment in bioavailability and half-life of DL-HPLA-BT PNPs than pure drug, impelled that this approach may be beneficial for targeting breast cancer. Although only few targeted drugs have been developed so far, this area is in constant growth and we strongly believe that this approach could give an added value to cancer therapy.

#### CRediT authorship contribution statement

**Sarita Rani:** Conceptualization, Methodology. **Rakesh K. Sahoo:** Methodology. **Kartik T. Nakhate:** Methodology. **Ajazuddin:** Methodology. **Umesh Gupta:** Conceptualization, Writing - review & editing.

#### Declaration of Competing Interest

The authors declare that they have no known competing financial interests or personal relationships that could have appeared to influence the work reported in this paper.

#### Acknowledgement

The authors acknowledge the financial support from the University Grants Commission, New Delhi, India and Department of Science and Technology, New Delhi, India through DST Start up Research Grant (Young Scientists) to Dr. Umesh Gupta. We are thankful to Fresenius Kabi Pvt. Ltd. for providing Bortezomib as a gift sample.

#### Appendix A. Supplementary material

Supplementary data to this article can be found online at <https://doi.org/10.1016/j.ijpharm.2020.119173>.

#### References

- Ringsdorf, H., 1975. Structure and properties of pharmacologically active polymers. *J. Polym. Sci. Polym. Symp.* 51, 135–153.
- Vasey, P.A., Kaye, S.B., Morrison, R., Twelves, C., Wilson, P., Duncan, R., Thomson, A.H., Murray, L.S., Hilditch, T.E., Murray, T., Burtles, S., Fraier, D., Frigerio, E., Cassidy, J., 1999. Phase I clinical and pharmacokinetic study of PK1 [N-(2-Hydroxypropyl) methacrylamide copolymer doxorubicin]: first member of a new class of chemotherapeutic agents-drug-polymer conjugates. cancer research campaign phase I/II committee. *Clin. Cancer Res.* 83–94.
- Baka, S., Clamp, A.R., Jayson, G.C., 2006. A review of the latest clinical compounds to inhibit VEGF in pathological angiogenesis. *Exp. Opin. Therapeut. Targets* 10, 867–876.
- Veronese, F.M., Pasut, G., 2005. Pegylation, successful approach to drug delivery. *Drug Discov. Today* 10, 1451–1458.
- Elsabahy, M., Wooley, K.L., 2012. Design of polymeric nanoparticles for biomedical delivery applications. *Chem. Soc. Rev.* 41, 2545–2561.
- Bray, F., Ferlay, J., Soerjomataram, I., Siegel, R.L., Torre, L.A., Jemal, A., 2018. Global Cancer Statistics: GLOBOCAN Estimates of Incidence and Mortality Worldwide for 36 Cancers in 185 Countries. *CA: Cancer J. Clin.* 68, 394–424.
- Chen, D., Frezza, M., Schmitt, S., Kanwar, J., Dou, Q.P., 2011. Bortezomib as the first proteasome inhibitor anticancer drug: current status and future perspectives. *Curr. Cancer Drug Targets* 11, 239–253.
- Papandreou, C.N., Daliani, D.D., Nix, D., Yang, H., Madden, T., Wang, X., 2004. Phase I trial of the proteasome inhibitor bortezomib in patients with advanced solid tumors with observations in androgen-independent prostate cancer. *J. Clin. Oncol.* 22, 2108–2121.
- Maynadier, M., Basile, I., Gallud, A., Gary-Bobo, M., Garcia, M., 2016. Combination treatment with proteasome inhibitors and antiestrogens has a synergistic effect mediated by p21WAF1 in estrogen receptor-positive breast cancer. *Oncol. Rep.* 36, 1127–1134.
- Thaler, S., Schmidt, M., Robetawag, S., Thiede, G., Schad, A., Sleeman, J.P., 2017. Proteasome inhibitors prevent Bi-directional HER2/estrogen-receptor cross-talk leading to cell death in endocrine and lapatinib-resistant HER2+/ER+ breast cancer cells. *Oncotarget* 8, 72281–72301.
- Xia, X., Liao, Y., Guo, Z., Li, Y., Jiang, L., Zhang, F., Chuyi, H., Yuan, L., Xuejun, W., Ningning, L., Jinbao, L., Hongbiao, H., 2018. Targeting roeasome-associated deubiquitinases as a novel strategy for the treatment of estrogen receptor-positive breast cancer. *Oncogenesis* 7, 75.
- Wei, W., Yue, Z.G., Qu, J.B., Yue, H., Su, Z.G., Ma, G.H., 2010. Galactosylated nanocrystallites of insoluble anticancer drug for liver-targeting therapy: an *in vitro* evaluation. *Nanomedicine* 5, 589–596.
- Su, J., Chen, F., Cryns, V.L., Messersmith, P.B., 2011. Catechol polymers for pH-responsive, targeted drug delivery to cancer cells. *J. Am. Chem. Soc.* 133, 11850–11853.
- Medel, S., Syrova, Z., Kovacic, L., Hrdy, J., Hornacek, M., Jager, E., Hruby, M., Lund, R., Cmarko, D., Stepanek, P., Raska, I., Nystromet, B., 2017. Curcumin-bortezomib loaded polymeric nanoparticles for synergistic cancer therapy. *Eur. Polym. J.* 93, 116–131.
- Duncan, R., 2009. Development of HPMA copolymer-anticancer conjugates: clinical experience and lessons learnt. *Adv. Drug Deliv. Rev.* 61, 1131–1148.
- Seymour, L.W., Ferry, D.R., Kerr, D.J., Rea, D., Whitlock, M., Poyner, R., Boivin, C., Hesselwood, S., Twelves, C., Blackie, R., Schatzlein, A., Jodrell, D., Bissett, D., Calvert, H., Lind, M., Robbins, A., Burtles, S., Duncan, R., Cassidy, J., 2009. Phase II studies of polymer-doxorubicin (PK1, FCE28068) in the treatment of breast lung and colorectal cancer. *Int. J. Oncol.* 34, 1629–1636.
- Barz, M., Arminan, A., Canal, F., Wolf, F., Koynov, K., Frey, H., 2012. P(HPMA)-block-P(LA) copolymers in paclitaxel formulations: poly(lactide) stereochemistry controls micellization cellular uptake kinetics, intracellular localization and drug efficiency. *J. Controll. Release* 163, 63–74.
- Senior, J., Crawley, J.C., Gregoriadis, G.G., 1985. Tissue distribution of liposomes exhibiting long half-lives in the circulation after intravenous injection. *Biochim. Biophys. Acta* 839, 1–8.
- Maiti, S., Park, N., Han, J.H., Jeon, H.M., Lee, J.H., Bhuniya, S., 2013. Gemcitabine-coumarin-biotin conjugates: a target specific theranostic anticancer prodrug. *J. Am. Chem. Soc.* 135, 4567–4572.
- Kue, C.S., Kamkaew, A., Burgess, K., Kiew, L.V., Chung, L.Y., Lee, H.B., 2016. Small molecules for active targeting in cancer. *Medi. Res. Rev.* 36, 494–575.

- Ren, W.X., Han, J., Uhm, S., Jang, Y.J., Kang, C., Kim, J.H., Kim, J.S., 2015. Recent development of biotin conjugation in biological imaging sensing, and target delivery. *Chem. Commun.* 51, 10403–10418.
- Shen, S., Xiao-Jiao, D., Liu, J., Rong, S., Zhu, Y.H., Wang, J., 2015. Delivery of bortezomib with nanoparticles for basal-like triple-negative breast cancer therapy. *J. Control. Release* 8, 14–24.
- Chytil, P., Etrych, T., Kriz, J., Subr, V., Ulbrich, K.K., 2010. N-(2-Hydroxypropyl) methacrylamide-based polymer conjugates with pH-controlled activation of doxorubicin for cell-specific or passive tumour targeting synthesis by RAFT polymerisation and physicochemical characterisation. *Eur. J. Pharm. Sci.* 41, 473–482.
- Upadhyay, S., Khan, I., Gothwal, A., Pachouri, P.K., Bhaskar, N., Gupta, U.D., 2017. Conjugated and entrapped HPMA-PLA nano-polymeric micelles based dual delivery of first line anti TB drugs: improved and safe drug delivery against sensitive and resistant mycobacterium tuberculosis. *Pharm. Res.* 34, 1944–1955.
- Hou, X., Wei, W., Fan, Y., Zhang, J., Zhu, N., Hong, H., 2017. Study on synthesis and bioactivity of biotinylated emodin. *Appl. Microbiol. Biotechnol.* 101, 5259–5266.
- Goodreid, J.D., Duspara, P.A., Bosch, C., Batey, R.A., 2014. Amidation reactions from the direct coupling of metal carboxylate salts with amines. *J. Org. Chem.* 79, 943–954.
- Getlik, M., Wilson, B.J., Morshed, M.M., Watson, I.D.G., Tang, D., Subramanian, P., 2013. Rearrangement of 4-Amino-3-halo-pyridines by nucleophilic aromatic substitution. *J. Org. Chem.* 78, 5705–5710.
- Pearce, S.T., Jordan, V.C., 2004. The biological role of estrogen receptors alpha and beta in cancer. *Crit. Rev. Oncol./Hematol.* 50, 3–22.
- Prabu, P., Chaudhari, A.A., Dharmaraj, N., Khil, M.S., Park, S., Kim, H.Y., 2009. Preparation, characterization, *in-vitro* drug release and cellular uptake of poly(capro lactone) grafted dextran copolymeric nanoparticles loaded with anticancer drug. *J. Biomed. Mater. Res. Part A* 90, 1128–1136.
- Rosca, I.D., Watari, F., Uo, M., 2004. Microparticle formation and its mechanism in single and double emulsion solvent evaporation. *J. Control. Release* 99, 271–280.
- Kumar, R.B., Rao, S.T., 2012. AFM studies on surface morphology topography and texture of nanostructured zinc aluminum oxide thin films. *J. Nano-mater. Biostruct.* 7, 1881–1889.
- Byrn, S.R., Tishmack, P.A., Milton, M.J., Van de Velde, H., 2011. Analysis of two commercially available bortezomib products: differences in assay of active agent and impurity profile. *AAPS Pharmaceut. Sci. Technol.* 12, 461–467.
- Kamalzadeh, Z., Babanezhad, E., Ghaffari, S., Mohseni-Ezhiyeh, A., Mohammadnejad, M., Naghibfar, M., Bararjanian, M., Attar, H., 2017. Determination of bortezomib in API samples using HPLC: assessment of enantiomeric and diastereomeric impurities. *J. Chromatogr. Sci.* 55, 697–705.
- Gupta, A., Ahmad, A., Singh, H., Kaur, S.K.M.N., Ansari, M.M., 2018. Nanocarrier composed of magnetite core coated with three polymeric shells mediates LCS-1 delivery for synthetic lethal therapy of BLM-defective colorectal cancer cells. *Biomacromolecules* 19, 803–815.
- Codony-Servat, J., Tapia, M.A., Bosch, M., Oliva, C., Domingo-Domenech, J., Mellado, B., 2006. Differential cellular and molecular effects of bortezomib, a proteasome inhibitor, in human breast cancer cells. *Mol. Cancer Ther.* 5, 665–675.
- Yang, W., Cheng, Y., Xu, T., Wang, X., Wen, L.P., 2009. Targeting cancer cells with biotin-dendrimer conjugates. *Eur. J. Med. Chem.* 44, 862–868.
- Doerflinger, A., Quang, N.N., Gravel, E., Pinna, G., Vandamme, M., Duconge, F., 2018. Biotin-functionalized targeted polydiacetylene micelles. *Chem. Commun.* 54, 3613–3616.
- Nie, J., Cheng, W., Peng, Y., Liu, L., Chen, Y., Wang, X., Liang, C., Tao, W., Wei, Y., Zeng, X., Mei, L., 2017. Co-delivery of docetaxel and bortezomib based on a targeting nanoplatfrom for enhancing cancer chemotherapy effects. *Drug Deliv.* 24, 1124–1138.
- Torchilin, V., 2011. Tumor delivery of macromolecular drugs based on the EPR effect. *Adv. Drug Deliv. Rev.* 63, 131–135.
- Y. Singh, K.K.D.R. Viswanadham, V.K. Pawar, J. Meher, A.K. Jajoriya, A. Omer, S. Jaiswal, J. Dewangan, H.K. Bora, P. Singh, S.K. Rath, L. Jawahar, D.P. Mishra, M.K. Chourasia, M.K. Induction of Mitochondrial Cell Death and Reversal of Anticancer Drug Resistance via Nanocarriers Composed of a Triphenylphosphonium Derivative of Tocopheryl Polyethylene Glycol Succinate, *Mol. Pharmaceut.* (2019). DOI 10.1021/acs.molpharmaceut.9b00177.
- Vineberg, J.G., Zuniga, E.S., Kamath, A., Chen, Y.J., Seitz, J.D., Ojima, I., 2014. Design, synthesis, and biological evaluations of tumor-targeting dual-warhead conjugates for a taxoid – camptothecin combination chemotherapy. *J. Med. Chem.* 57, 5777–5791.